Indian Journal of Chemical Technology
Vol. 33, January 2026, pp. 94-109
DOI: 10.56042/ijct.v33i1.18899

Pioneering degradation of acid blue 113 dye with photocatalysis and bioremediation in a novel sequential reactor

Vaibhav Kumar Rai[1], Sudeep Yadav[3], Himanshu Tiwari[2] & Ram Sharan Singh[2]*

[1]Department of Chemical Engineering, Bipin Tripathi Kumaon Institute of Technology, Dwarahat 263653, Uttarakhand, India

[2]Department of Chemical Engineering & Technology, Indian Institute of Technology (BHU), Varanasi 221005, Uttar Pradesh, India

[3]Department of Chemical Engineering, Bundelkhand Institute of Engineering & Technology, Jhansi 284128, Uttar Pradesh, India

*E-mail: rssingh.che@itbhu.ac.in

Received 18 April 2025; accepted 18 December 2025

In this study, a novel approach is elucidated by utilizing a synergistic combination of photocatalytic oxidation and bioremediation for the degradation of Acid Blue 113 dye. TiO_2/GO composite is employed as a photocatalyst in the photocatalytic reactor, while polyurethane foam is used as packing media to immobilize the microbes in a fixed bed bioreactor. TiO_2/GO composite has been prepared using a one-step hydrothermal technique and characterized through FTIR, HR-XRD, SEM, and BET analyses, revealing its structural and morphological properties. The energy band gap of the composite is determined to be 2.73 eV. Preliminary photocatalytic oxidation of the Acid Blue 113 dye demonstrated a notable improvement in the biodegradability index (BOD/COD = 0.416 ± 0.0128) and a significant reduction in the permanganate index (66.18%). Furthermore, the application of a fixed bed bioreactor proved highly effective in mitigating dye loading stress and exhibited excellent dye biodegradation efficiency. The bioreactor system demonstrated its remarkable capability of 85.03 ± 2.76% biodegradation of the dye loading of 700 mg/L. Additionally, residual toxicity assessment ensured the safe disposal of the treated dye wastewater into the environment.

Keywords: Fixed bed bioreactor, Hydrothermal method, Permanganate Index, Photocatalytic reactor, TiO_2/GO composite

Introduction

The textile industry proliferates globally as the market demand surges, emanating enormous amounts of dyeing wastewater. Recent technological development brings a revolution in the production of various synthetic dyes. These dyes adversely affect the survival of aquatic life and living being due to poor wastewater management and disposal of untreated wastewater into the environment[1]. The emission of various recalcitrant dyes leads to severe health issues including cyanosis, urinary bladder cancer, immune suppression, DNA damage, allergic dermatitis, and apoptosis[2,3]. A World Bank study found that the textile industry is responsible for around 17% of water contamination; furthermore, 10 to 15 percent of the dye-containing water is released into natural water sources without being treated[4]. In addition, the textile sector is one of the most water-intensive industries, using 0.4 m^3/kg of fresh water or 2.1% of all used industrial water[5]. Additionally, it is anticipated that the per capita demand for textiles would continue to rise. Controlling the pollution brought on by the release of untreated textile wastewater into the environment is one of the global goals[6]. Considering the threat of vanishing aquatic life cycle, environment pollution, and severe impact on human health, an effective technique is highly desirable for the treatment of synthetic dyes.

Acid Blue 113 (AB 113), a bis-azo dye, is ubiquitously used in textile industry for silk, cotton, polyamide fibers, acrylic fibers, and wool dyeing[7]. The presence of two azo bonds profoundly makes it recalcitrant, hence difficult to biodegrade. Since microorganisms sometimes face difficulty to survive and may reach the verge of dormancy where their metabolic activity decreases, however, their cells are alive in the environment of recalcitrant organic pollutants[8]. Preliminary treatment is therefore vital to enhance the biodegradability index (BOD/COD) and facilitate biodegradation of AB 113[9]. Numerous advanced oxidation processes (AOPs)[10,11] such as Fenton oxidation, ozonation, photo-Fenton process, ultrasonic treatment, γ-radiolysis, and photocatalytic oxidation are preliminary employed for the treatment of textile wastewater. Hence, a suitable combination of AOP along with bioremediation (i.e., hybrid technique) can profoundly be useful for the complete mineralization of AB 113.

Photocatalytic oxidation has widespread application for the treatment of recalcitrant organic compounds, especially for dyes[12]. In wastewater treatment, anatase Titanium(IV) oxide (TiO_2) is a more suitable photocatalyst due to its chemical stability, high photocatalytic activity[13], non-toxic nature, environmentally friendly, and good optical properties[14]. Meanwhile, a wide energy bandgap (3.2 eV), UV-assisted photocatalytic activity, low quantum yield, low activity in visible light, and rapid recombination of photo-generated e^-/h^+ pairs restrict its applications for wastewater treatment[15]. Graphene Oxide (GO) is used as a loading material to proliferate the photocatalytic activity of TiO_2 under visible range and mitigate the recombination of e^-/h^+ pairs[12]. GO possesses high conductivity, electron transfer efficacy, large surface area, mechanical strength, and good adsorption property[16]. A composite of TiO_2 and GO (TiO_2/GO) significantly enhance the photocatalytic activity due to its low energy bandgap and promptly segregate the charge carrier at the interface of GO. The narrow band gap will increase the rate of electron charge transfer[17]. The one-step hydrothermal technique used for the synthesis of the TiO_2/GO composite photocatalyst is a well-known method for preparing composite materials with enhanced properties. The hydrothermal process allows for the formation of strong chemical bonds between the TiO_2 nanoparticles and the GO sheets, resulting in the formation of a composite material with synergistic properties, such as improved photocatalytic activity due to the combined effects of TiO_2 and GO[18].

The photocatalytic oxidized products have toxicity and further require the post-treatment before its disposal into the environment[19]. Bioremediation is a liable and environmentally friendly technique for the complete degradation and detoxification of dye and its intermediate compounds[20]. A post-biological treatment of photocatalytically oxidized AB 113 might be an efficient hybrid technique for complete mineralization.

The central hypothesis of this work is that photocatalytic AOP pretreatment using TiO_2/GO can transform complex azo dye molecules into smaller, less toxic, and more biodegradable intermediates, thereby enhancing microbial uptake in the FBR. By bridging oxidative cleavage with biofilm-driven mineralization, the hybrid system is expected to deliver superior degradation efficiency and reduced HRT compared to standalone processes.

The present work elucidates the degradation study of AB 113 through a combination of photocatalytic oxidation and biodegradation. The efficacy of GO doped TiO_2/GO photocatalyst was examined using the UV-visible spectroscopy. The performance of fixed bed bioreactor was analysed based on the inlet dye loading. FTIR, HR-XRD, SEM, and BET were carried out to evaluate the functional group, phase composition, surface morphology, and surface area, respectively. The residual toxicity assessment was also carried out to ensure the complete detoxification of treated wastewater.

Experimental Section

Dye and chemicals

Acid Blue 113 ($C_{32}H_{21}N_5Na_2O_6S_2$) dye, Anatase Titanium (IV) oxide, Graphite powder, Sodium nitrate ($NaNO_3$), Potassium permanganate ($KMnO_4$), Hydrogen peroxide (H_2O_2), Di-Ammonium oxalate monohydrate, Sodium oxalate, t-Butyl alcohol, Benzoquinone, and Sulfuric acid (H_2SO_4) were obtained from Sigma Aldrich (India). The mineral salt media (MSM) composition were as follows (g/L): KH_2PO_4 (1.05), K_2HPO_4 (1.6), $(NH_4)_2SO_4$ (0.5), NaCl (2), $CaCl_2{\cdot}2H_2O$ (0.3), $MgSO_4{\cdot}7H_2O$ (0.2), $MnSO_4{\cdot}H_2O$ (0.01), $FeSO_4{\cdot}7H_2O$ (0.03), biopeptone (1.0), and glucose (1.0).

Graphene oxide (GO) and TiO_2/GO composite preparation

Graphene oxide (GO) was prepared using the Modified Hummers' method[21,22]. The procedure involved mixing Graphite powder (2.0 g), $NaNO_3$ (2.0 g), and H_2SO_4 (98% purity) (90 mL) in an Erlenmeyer flask, which was placed under an ice bath (0-5 °C). The mixture was then magnetically stirred for 4 h, followed by the slow addition of 12 g of $KMnO_4$ to the reaction mixture, ensuring that the temperature of the solution remained below 15°C. The mixture was stirred for another 2 h. The ice bath was removed, and the mixture was allowed to heat up to 35°C for 2 h. After that, 180 mL of distilled water was added to the mixture, and it was constantly stirred while being heated (not boiled) at 95°C for 1 h. The heater was turned off, and the mixture was allowed to cool down at room temperature (27°C). Further, 100 mL of deionized water was added to the beaker, followed by the addition of 60 mL of H_2O_2 (30% v/v) to the mixture, which was then stirred for another 30 min. The resulting mixture was centrifuged at 4000 rpm for 10 min (REMI CENTRIFUGE,

RM- 12C BL), and the supernatant was discarded. The remaining sediment was washed several times with 1 M HCl solution and then with deionized water until the pH of the solution was neutral. Finally, the sediment was dried in an oven at 60°C for 24 h to obtain GO powder.

A one-step hydrothermal method was used to synthesize TiO_2/GO (95:5) composite photocatalyst[4]. The choice of this composition is consistent with literature findings that introducing a small amount of GO (5–10%) into a TiO_2 matrix significantly enhances photocatalytic performance by providing additional electron-transport pathways, suppressing electron–hole recombination, and extending visible-light absorption[23]. Briefly, 0.05 g of GO was re-exfoliated in 30 mL of ethanol by ultrasonic treatment for 2 h (Model- U.C. SW-4, Ultrasonic bath). Next, 1.0 g of TiO_2 nanoparticles was added into 70 mL of double-distilled water and stirred until a homogeneous solution was obtained. The GO and TiO_2 mixture were exposed to ultrasonication for 45 min to obtain a uniform solution. This solution was placed in a Teflon-lined autoclave and kept at 170°C for 2 hr. The resulting composite was recovered by centrifugation (5000 rpm, 10 min), rinsed with deionized water, and oven dried at 90°C for 10 h. The calcination was carried out at 400°C to enhance the photocatalytic properties of the composite and promote the growth and crystallization of TiO_2 nanoparticles. Calcination helps to remove any residual organic content, which can improve the purity and stability of the composite material. Additionally, the crystallization of TiO_2 nanoparticles during calcination can enhance their surface area and light absorption properties, leading to improved photocatalytic efficiency.

Microorganism

In this study, the biodegradation of AB 113 was carried out using a promising bacterial species, *Klebsiella michiganensis* strain DP2ZMA43 (Accession No. MH972172)[9]. Detailed information regarding the bacterial species, including its taxonomic classification, and physiological characteristics, provided in the Supplementary Information.

Characterization

TiO_2/GO composite was thoroughly characterized using advanced analytical instruments, including Fourier transform infrared spectroscopy (FTIR) (Nicolet iS5, resolution of 4 cm^{-1}, 32 scans), High-Resolution X-Ray diffraction (HR-XRD) (Rigaku SmartLab 9kW, $\lambda_{CuK\alpha}$ = 0.15418 nm), Brunauer-Emmett-Teller (BET) surface area analysis (MicrotracBEL), and Scanning electron microscopy (SEM) (ZEISS EVO-MA15/18). The characterization techniques employed provided a comprehensive understanding of the composition, structure, and morphology of the prepared photocatalyst, (i.e., TiO_2/GO composite). Permanganate Index (PI) of AB 113 was analyzed based on the standard titration based method mentioned elsewhere[24]. Chemical Oxygen Demand (COD) and Biochemical Oxygen Demand (BOD) of AB 113 were measured using the standard protocol. Total Organic Carbon (TOC) of AB 113 wastewater was measured by TOC analyzer (multi N/C 2100/2100S, Analytikjena, Germany).

Photocatalytic potential of TiO_2/GO composite photocatalyst

Tauc plot is widely employed to determine the energy band gap of semiconducting materials. It is based on the Tauc equation, which relates the absorption coefficient (α) to the energy (E_g) of a photon through the expression $\alpha \propto (h\nu - E_g)^{n}$, where $h\nu$ is the photon energy (eV), E_g is the energy band gap (eV), and n is a constant that depends on the nature of the transition (typically $n = \frac{1}{2}$ or 2). In the Tauc plot, the square root of the absorption coefficient $[(\alpha h\nu)^{\frac{1}{2}}]$ was plotted against the photon energy $(h\nu)$[(Ref.25)]. This plot allowed for a visual determination of the energy band gap, which was represented by the extrapolated linear portion of the plot intersecting the x-axis.

For indirect transition ($n = \frac{1}{2}$), the final equation for Tauc plot is as follows:

$$(\alpha h\nu)^{\frac{1}{2}} = K\,(h\nu - E_g) \quad \ldots (1)$$

Where, α is the optical absorption coefficient (cm^{-1}), $h\nu$ is the photon energy (eV), h is Planck's constant (J s), ν is the frequency (Hz or s^{-1}), E_g is the optical band gap (eV), n depends on the type of electronic transition in the material, for direct band gaps, $n = \frac{1}{2}$, and for indirect band gaps, n = 2, and K(cm^{-1}/eV) represents the energy independent constant.

Photon energy $h\nu$ (eV) can be obtained from wavelength λ (nm) by Eq. 2.

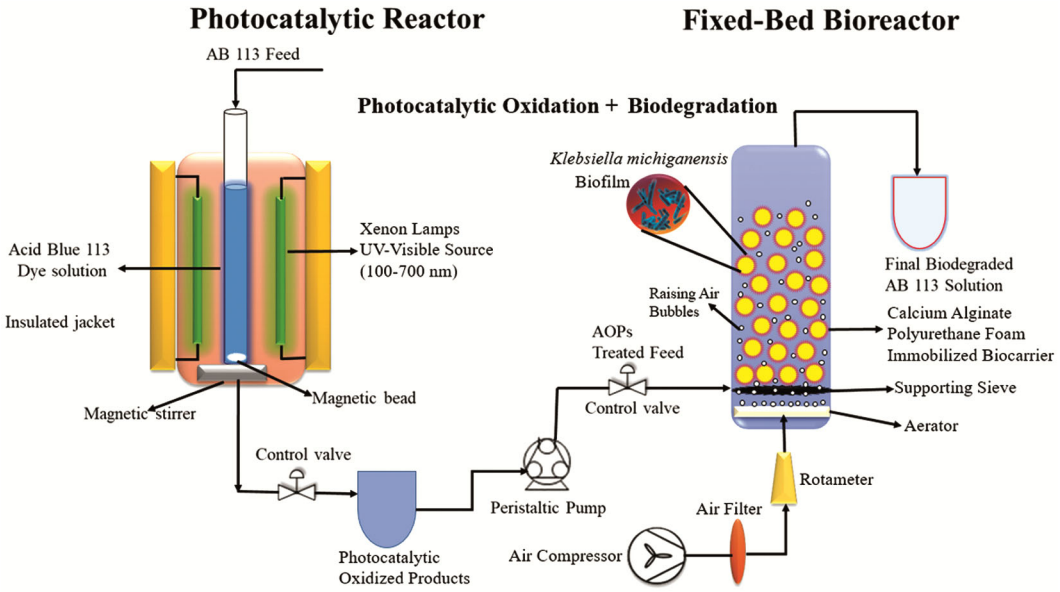

Fig. 1 — Schematic illustration of photocatalytic reactor and fixed bed bioreactor, indigenously designed laboratory-scale sequential reactor setup for the remediation of Acid Blue 113 dye

$$h\nu(\text{eV}) = \frac{1240}{\lambda\,(\text{nm})} \quad \ldots (2)$$

Experimental laboratory scale reactor setup

Photocatalytic reactor (PCR)

A laboratory-scale Photocatalytic Reactor (PCR) was used to investigate the performance of the synthesized TiO_2/GO composite photocatalyst. The semi-batch reactor was designed of quartz glass with a capacity of 200 mL (Fig. 1). The PCR was equipped with a Xenon lamp (150 W) that provided the necessary UV-visible light spectrum (100-700 nm), having light intensity at the reactor surface within 18–22 mW/cm² for the photocatalytic reactions to occur. The light intensity was determined using a calibrated digital radiometer (Analytik Jena 97-0015-02(UVX)). A magnetic stirrer was used to agitate the solution to ensure efficient mixing and uniform illumination of the TiO_2/GO composite photocatalyst. The pH of the solution was maintained at 7.0±0.5 using 0.1 M NaOH or 0.1 M HCl solutions. The entire reactor assembly was insulated to minimize heat loss and maintain a stable operating temperature. The composite photocatalyst was recovered at the end of each experiment through centrifugation (5000 rpm, 15 min) followed by vacuum drying at 80 °C for 3 h duration.

Fixed Bed Bioreactor (FBR)

A laboratory-scale Fixed Bed Bioreactor (FBR) was designed to investigate the biodegradation of photocatalytically oxidized AB 113 solution. The bioreactor had an active volume of 800 mL and was packed with polyurethane foam (PU Foam) as a support media for the immobilized bacterial species, *Klebsiella michiganensis* (Fig. 1). The diameter and height of FBR were 6 cm and 100 cm, respectively. The bacterial immobilization method involved the use of a calcium alginate matrix, which was used to encapsulate the bacterial cells and attach them to the polyurethane foam packing material. To immobilize the bacterial species, an active culture of *Klebsiella michiganensis* (Optical Density $(OD)_{600}$ = 1) was grown in a nutrient broth medium and harvested by centrifugation (5000 rpm, 10 min). The bacterial pellets were then suspended in a solution of sodium alginate (2.5 wt%) and mixed thoroughly. The resulting mixture was then extruded through a syringe needle into a calcium chloride solution (6 wt%), where the alginate gel matrix formed around the bacterial cells, immobilizing them within the matrix. The calcium alginate matrix provided a protective environment for the bacterial cells and allowed for a high degree of bacterial cell attachment and growth on the PU foam[26]. The immobilized bacteria were then loaded into the polyurethane foam-packed bed of the bioreactor, and the photocatalytically oxidized AB 113 solution was fed into the reactor. The bioreactor unit distributed the substrate solution evenly across the packing material and maintained a constant flow rate. Before beginning the FBR, an acclimatization period of 15 days was allowed for the microbial

species to form a stable biofilm using an inoculum dose of 2×10^7 colony-forming units per millilitre (CFU/mL). The reactor was operated at a room temperature of 27 ± 3°C, with the dissolved oxygen (DO) content maintained in the range of 2.0 – 4.0 mg/L through continuous aeration, and an adjusted pH of 7 ± 0.5.

Toxicity assessment

The potential environmental impact of treated AB 113 wastewater can be assessed by evaluating the toxicity of the dye, as well as its photocatalytically oxidized (PO) and biodegradation products (BP), through microbial toxicity tests. In this study, bacterial cultures of *E. coli* (Gram-negative) and *Bacillus Subtilis* (Gram-positive) were utilized for toxicity assessment of AB 113 (200 mg/L) and its sequential degraded by-products. To prepare the bacterial cultures, both strains were grown overnight in nutrient broth media, and the log phase cultures were subsequently obtained through centrifugation (REMI CENTRIFUGE, RM- 12C BL, 4500 rpm, 20 min). The log phase cell pellets of both strains were carefully washed with phosphate buffered saline (PBS) to eliminate any remaining nutrients. The resulting cell pellets, with a concentration of 10^7 CFU/mL, were used to prepare bacterial cultures in nutrient broth for residual toxicity assessment. For the toxicity assessment, double distilled water was used as a reference, while AB 113, PO, and BP were exposed to the two bacterial cell culture media for duration of 24 h. The cellular viability of each sample was analyzed using a conventional plate count test, as described in a previous study[27]. The viability of the treated cells was estimated by comparing with control samples.

Pseudo-first-order model (apparent kinetics)

The observed substrate removal was determined using an apparent first-order expression:

$$-R_p = \frac{dC}{dt} = -k_{app}\, C \qquad \ldots (3)$$

For a contact time equal to the hydraulic retention time (HRT, t), the relation between influent concentration C_{in}, effluent concentration C_{out} and the apparent rate constant k_{app} (day^{-1}) is:

$$ln\left(\frac{C_{in}}{C_{out}}\right) = k_{app}(\mathrm{HRT}) \qquad \ldots (4)$$

Therefore, the apparent rate constant k_{app} can be calculated by the following mathematical expression:

$$k_{app} = \frac{1}{HRT}\, ln\left(\frac{C_{in}}{C_{out}}\right) \qquad \ldots (5)$$

Results and Discussion

Characterization

FTIR spectral analysis

The FTIR spectral analysis of synthesized GO exhibited a broad peak at 3407.5 cm^{-1}, attributed to the stretching vibration of hydroxyl (-OH) groups, while the peak at 1717.9 cm^{-1} corresponds to the stretching vibration of carbonyl (C=O) groups, indicating the presence of oxygen-containing functional groups on the GO surface[28] (Fig. 2). The peaks at 1594.25 and 1050.05 cm^{-1} were associated to the stretching vibrations of aromatic C=C and epoxy groups (C-O-C) groups, respectively, confirming the presence of graphene-like structure in GO[29]. The peak at 1228 cm^{-1} was attributed to the stretching vibration of alkoxy ($-OCH_3$) or hydroxyl (-OH) groups, indicating the presence of oxygen-containing functional groups on the edges of GO sheets. The presence of these functional groups indicated the successful oxidation of graphene to form GO.

The FTIR spectrum of TiO_2 exhibited the peak at 3420 cm^{-1} attributed to the stretching vibration of hydroxyl (-OH) groups, while the peak at 1628 cm^{-1} corresponds to the bending vibration of adsorbed water molecules or hydroxyl (Ti-OH) groups on the TiO_2 surface[30]. The peaks at 743.6 and 586 cm^{-1} were assigned to the stretching vibrations of Ti-O and Ti-O-Ti bonds, respectively, indicating the presence of titanium-oxygen (Ti-O) bonds in TiO_2 crystal lattice[17].

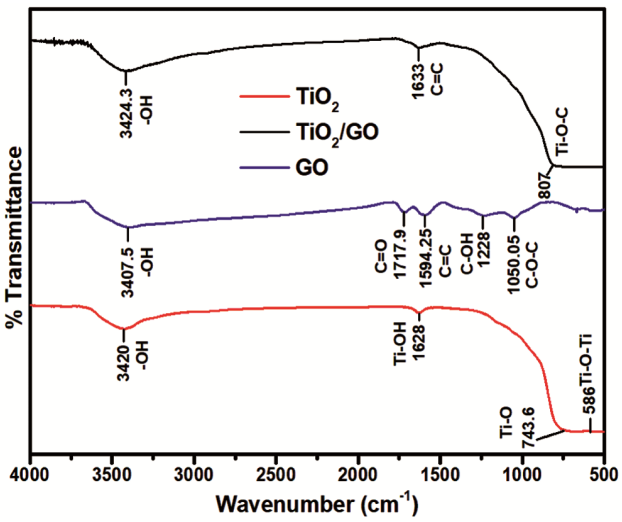

Fig. 2 — FTIR spectra of anatase Tio_2, GO and composite photocatalyst TiO_2/GO

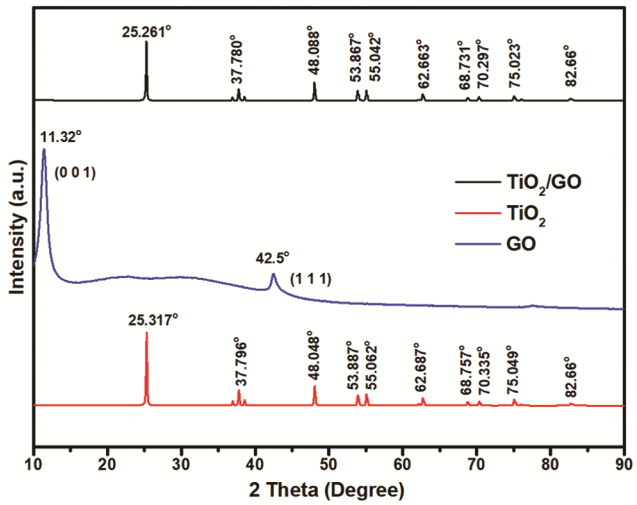

Fig. 3 —XRD analysis of GO, TiO_2 and TiO_2/GO composite photocatalyst

In the FTIR spectrum of the TiO_2/GO composite photocatalyst, peaks were observed at 3424.3, 1633, and 807 cm^{-1} wavenumber, corresponding to functional groups -OH, C=C, and Ti-O-C, respectively[23]. These peaks suggested that the composite material retained the characteristic functional groups of both GO and TiO_2. The presence of -OH groups indicated the hydroxyl groups on the surface of TiO_2, while the peak at 1633 cm^{-1} was attributed to the C=C stretching vibration of the graphene sheets in GO[31]. The peak at 807 cm^{-1} was indicative of the Ti-O-C bond, which suggested that TiO_2 nanoparticles were attached to the surface of GO through chemical bonding, and could be liable for the enhanced photocatalytic properties of the composite material.

High-resolution X-ray diffraction (HR-XRD) analysis

The XRD plot of GO showed two characteristic peaks at 11.32° and 42.5° (Fig. 3). The observed peaks at 11.32° correspond to the (001) plane reflection, indicating the presence of a well-ordered graphene structure in GO. The peak at 42.5° can be attributed to the (111) plane reflection, indicating the stacking of graphene layers in GO. These peaks indicated the presence of a layered structure in GO, with a high degree of graphitization and oxygen-containing functional groups (such as -OH, -COOH, and -C=O) on the surface[17].

The XRD plot of TiO_2 exhibited several peaks at 25.317°, 37.796°, 48.048°, 53.887°, 55.062°, 62.687°, 68.757°, 70.335°, 75.049°, and 82.66°, corresponding to the anatase crystal structure (101), (004), (200), (105), (211), (204), (116), (220), (215), and (224) planes, respectively, (JCPDS Card No. 21-1272)[32].

The XRD plot of the TiO_2/GO composite photocatalyst displayed similar peaks to those of TiO_2, indicating that the anatase phase was still present in the composite[12]. However, the intensities and positions of the peaks were slightly different, which suggested that the incorporation of GO had affected the crystal structure and morphology of TiO_2 and preserved crystallographic integrity. This effect could be attributed to the strong interaction between TiO_2 and GO through chemical bonds and/or physical adsorption. These enhanced the electron transfer and separation efficiency and thereby improved the photocatalytic performance of the composite.

Scanning Electron Microscopy (SEM) and Energy Dispersive X-ray (EDX) analysis

In the SEM image of GO, it was observed that the sheets appeared thin, randomly aggregated, and crumpled, forming a disordered solid (Fig. 4a). The irregular shape of GO and its thin-layered structure with wrinkles suggested the presence of fold structures resulting from stacking, possibly due to the introduction of oxidizing functional groups[31,33]. Remarkably, the SEM micrograph of fabricated GO indicated the successful formation of a single layer of graphene oxide, as confirmed by the absence of multilayer structures. On the other hand, TiO_2 nanostructures displayed a uniform distribution and spherical shape, albeit in an agglomerated form[23] (Fig. 4b). Meanwhile, the TiO_2 aggregates were found to be present on the GO layers, likely due to the high surface area of the GO sheets leading to the formation of aggregated and crumpled surfaces[12] (Fig. 4c). Intriguingly, the SEM image of TiO_2/GO composite revealed a well-dispersed distribution of TiO_2 nanoparticles on the surface of the GO sheets, indicating successful loading of TiO_2 onto GO. However, the presence of TiO_2 agglomerates was also observed, due to the relatively higher amount of TiO_2 compared to the carbon nanosheets. The thin-layered, aggregated, and crumpled sheets of GO, along with the uniform distribution of TiO_2 nanoparticles on GO surfaces, provided valuable insights into the unique properties and potential applications of these materials in photocatalytic processes.

The EDX spectra revealed that GO exhibited a prominent peak corresponding to carbon (C) element, indicative of its high carbon content (Fig. 4d). TiO_2, on the other hand, displayed peaks for oxygen (O)

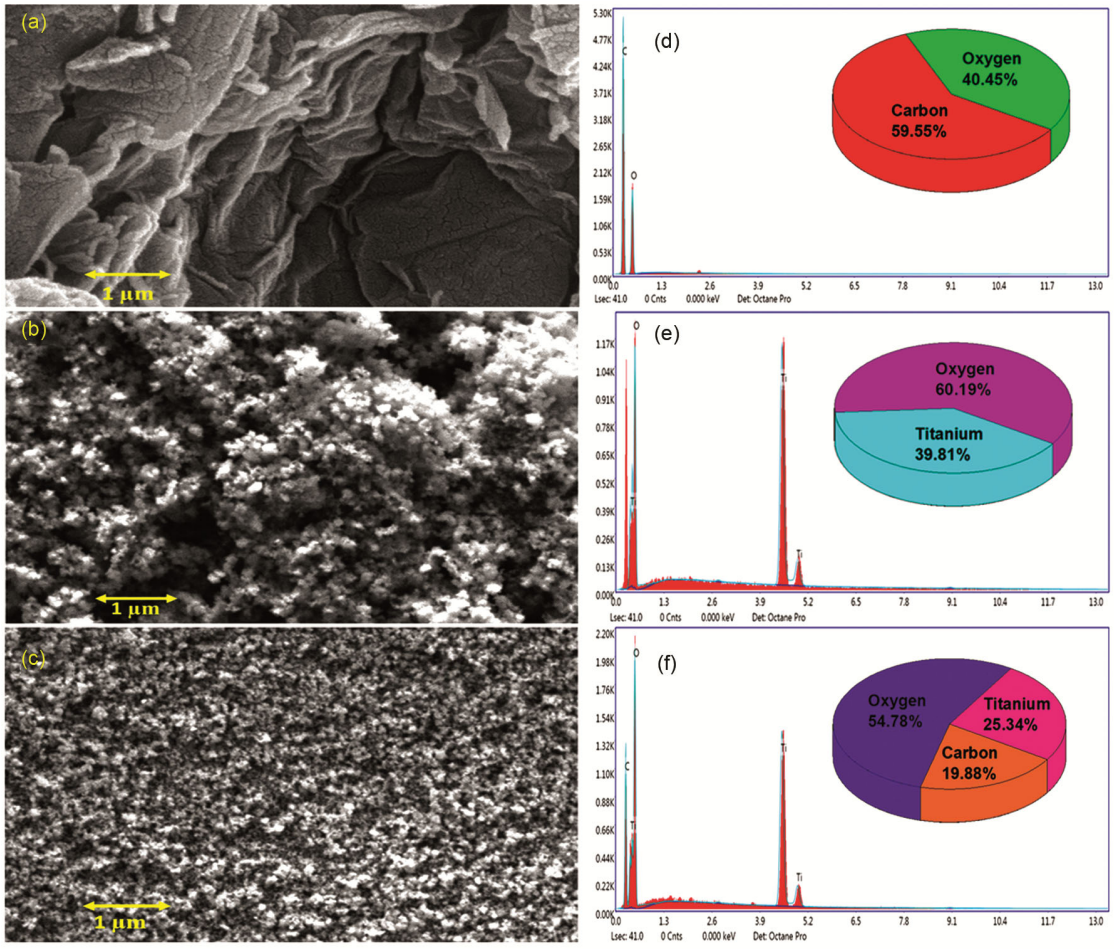

Fig. 4 — Morphology, elemental composition, and weight percentage distribution of Graphene Oxide, Titanium (IV) Oxide, and TiO_2/GO composite photocatalyst. (a-c) Scanning Electron Micrograph shows the morphology of (a) Graphene Oxide, (b) Anatase Titanium (IV) Oxide, and (c) TiO_2/GO composite. Energy Dispersive X-ray Spectroscopy spectra in (d-f) reveal the elemental composition and weight percentage distribution of (d) GO, (e) TiO_2, and (f) TiO_2/GO composite

and titanium (Ti) elements, suggesting the presence of these elements in its composition (Fig. 4e). In the case of TiO_2/GO nanocomposites, the EDX spectra exhibited peaks for all three elements - carbon (C), oxygen (O), and titanium (Ti), confirming the successful incorporation of GO into the TiO_2 crystal lattice (Fig. 4f). The intensity of the peaks in the spectrum provided insight into the relative concentration of each element. The quantitative analysis of the EDX spectra further revealed the weight percentage distribution of each element in the nanocomposites. These weight percentage distributions were calculated using the EDX spectrum, demonstrating the successful synthesis of the TiO_2/GO nanocomposite.

Brunauer-Emmett-Teller (BET) surface area

BET surface area findings of TiO_2 and TiO_2/GO composite photocatalysts reveal important insights into the structural properties of these nanoparticles and their potential for photocatalytic applications. Based on the experimental findings, BET surface area measurements of TiO_2 and TiO_2/GO composite photocatalysts were determined to be 10.315 and 12.033 m^2/g, respectively (Fig. 5a and 5b).The increase in specific surface area of the TiO_2/GO composite can be attributed to the presence of GO in the composite. GO is a two-dimensional nanomaterial with a large surface area due to its layered structure consisting of sp^2 hybridized carbon atoms arranged in a hexagonal lattice. The GO sheets are known to have a large number of functional groups, such as hydroxyl, epoxy, and carboxyl groups, which provides additional surface area for adsorption and reaction sites[34]. Therefore, the addition of GO to TiO_2 nanoparticles had led to an increase in the total surface area available for photocatalytic reactions,

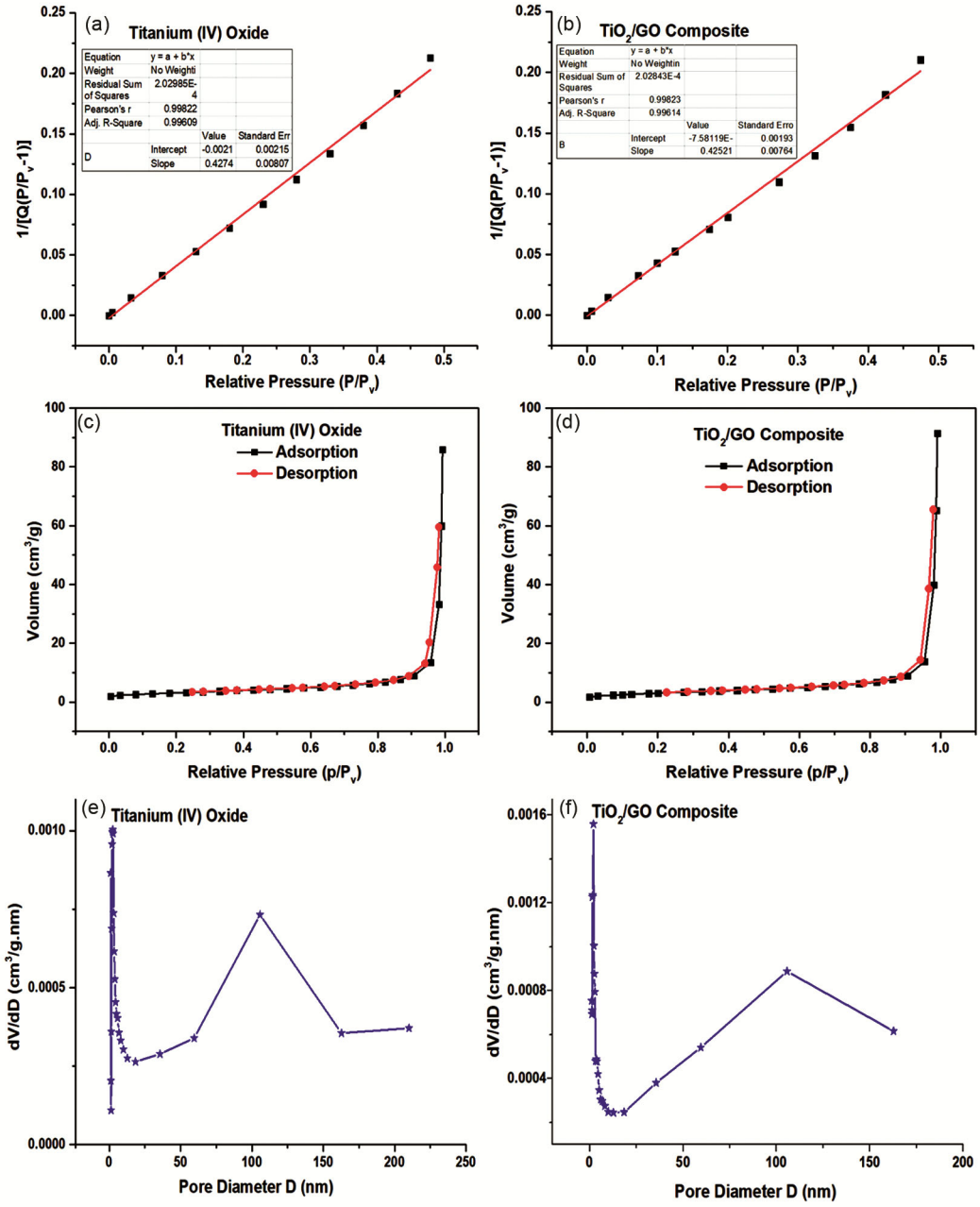

Fig. 5 — BET surface area analysis of (a) Titanium (IV) oxide and (b) TiO_2/GO composite photocatalyst. Hysteresis loops in N_2 adsorption/desorption isotherms for (c) TiO_2 and (d) TiO_2/GO composite; (e) Barrett-Joyner-Halenda (BJH) pore size distribution of TiO_2 and (f) TiO_2/GO composite

potentially enhancing the photocatalytic performance of the composite photocatalyst.

The average pore diameter of TiO_2 nanoparticles was measured to be 42.249 nm, while the average pore diameter of TiO_2/GO composite nanoparticles was found to be 39.495 nm (Fig. 5e,f). The decrease in pore diameter upon incorporation of GO can be attributed to the smaller size and thickness of GO compared to TiO_2 nanoparticles. The GO sheets, being only a few nanometers thick, can fill the larger pores of TiO_2 nanoparticles, resulting in a reduction in the average pore diameter in the TiO_2/GO composite. This phenomenon is further supported by the fact that GO sheets can form a closely packed structure, which can reduce the size of the pores in the composite photocatalyst. Additionally, the incorporation of GO into TiO_2 can also lead to the formation of mesopores in the TiO_2/GO composite, as GO sheets can act as

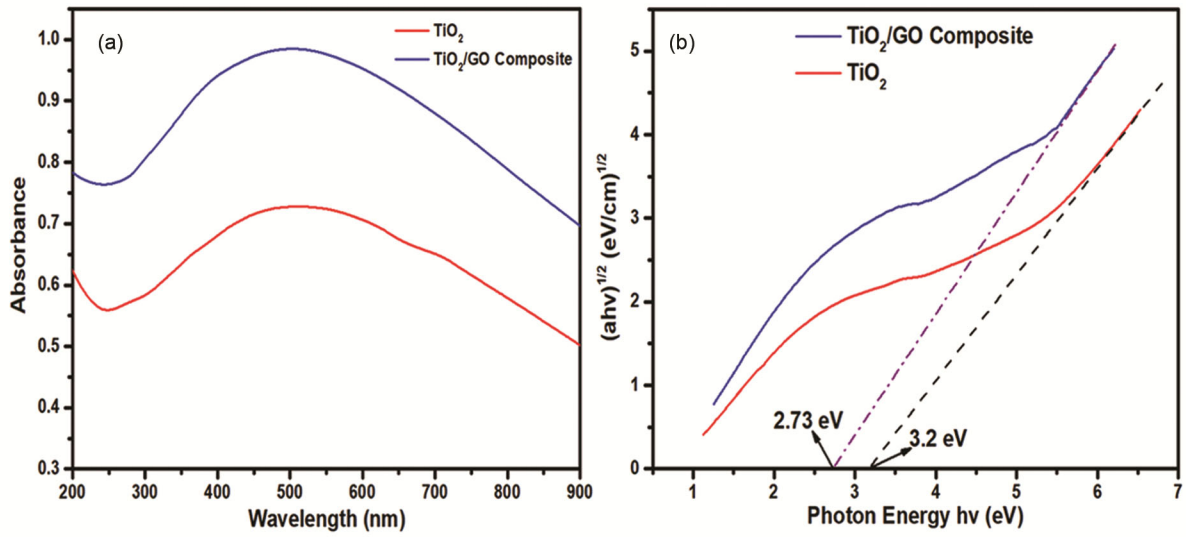

Fig. 6 — (a) UV-visible absorbance spectra revealing their distinct light absorption behaviors and (b) Tauc plots depict their photoactivity potential of TiO_2 and TiO_2/GO composite

spacers between TiO_2 nanoparticles, creating mesoporous channels (Fig. 5c,d). These mesopores can provide additional pathways for dye molecules to diffuse and reach the active sites on the TiO_2 surface, which can enhance the photocatalytic activity of the TiO_2/GO composite.

Tauc Plot: Energy band gap of TiO_2/GO composite photocatalyst

Tauc plot was drawn from the corresponding absorbance data to determine the energy band gaps (Fig. 6a). It was observed that the energy band gap of the TiO_2/GO composite photocatalyst (2.73 eV) was smaller than that of anatase TiO_2 (3.2 eV) (Eq. 1) (Fig. 6b). This indicated that the incorporation of GO into the TiO_2 matrix resulted in a reduced energy band gap, making the composite photocatalyst more sensitive to visible light. Since the incorporation of GO into the TiO_2 matrix may have caused a change in the electronic structure of the composite material. Graphene oxide is known to have a high electron density and can act as an electron donor. This could result in a decrease in the energy band gap of the composite photocatalyst. The additional electron density could lower the conduction band energy level, facilitating easier electron transitions and reducing the required energy for the transition (lower band gap)[35].

Moreover, the presence of GO in the TiO_2/GO composite photocatalyst could also enhance the light absorption properties of the material. GO has a broad absorption spectrum, covering a wide range of wavelengths from ultraviolet to visible light. This increased light absorption could result in a higher number of electrons being excited from the valence band to the conduction band, leading to a decrease in the energy band gap[34]. Furthermore, the formation of a heterojunction between TiO_2 and GO in the composite photocatalyst can create an additional energy level within the band gap, known as an energy trap or defect state. This energy may trap and localize charge carriers, thereby reducing the band gap and facilitating photocatalytic reactions. The previous study[9] employed pure TiO_2 with a band gap of 3.2 eV; the present finding introduces a TiO_2/GO composite with a significantly reduced band gap of 2.73 eV. The previous study was limited to the ultraviolet (UV light) spectrum; this study paved the path towards the incorporation of a broad spectrum to proliferate the photocatalytic efficacy.

The energy band gap of 3, 10, and 15 wt% of GO/TiO_2 composite photocatalyst were calculated[23] to be 3.06, 2.98, and 2.3 eV, respectively. Similarly, the lower energy band of 2.47 eV was obtained for the TiO_2/GO nanocomposite prepared via the liquid phase deposition technique[31]. Moreover, a varying energy band gap within the range of 2.35-2.80 eV has been reported for the TiO_2/GO composite photocatalyst, which somehow depends on the GO amount[34].

Photocatalytic reactor

Assessment of photocatalytic pretreatment of AB 113 Dye

Permanganate Index (PI) and Biodegradability Index (BI) are important indicators to evaluate the degree of degradation of organic compounds in

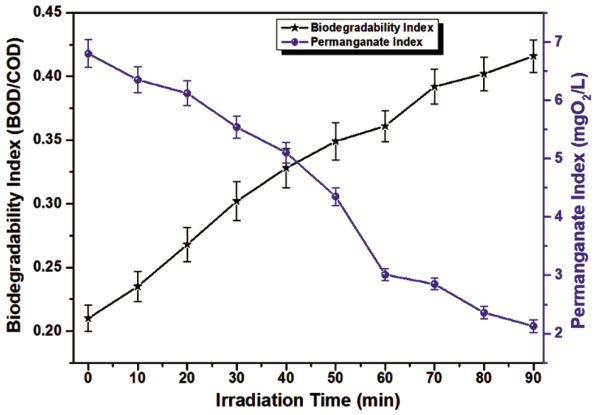

Fig. 7 — Demonstrating the dynamic changes in Biodegradability Index (BI) and Permanganate Index (PI) during the photocatalytic pretreatment of AB 113 dye (Dye concentration: 100 mg/L, TiO_2/GO composite: 0.5 g/L, pH: 7.0 ± 0.5, and ambient temperature: 27 ± 3 °C, Error bars represent the standard error of triplicate studies)

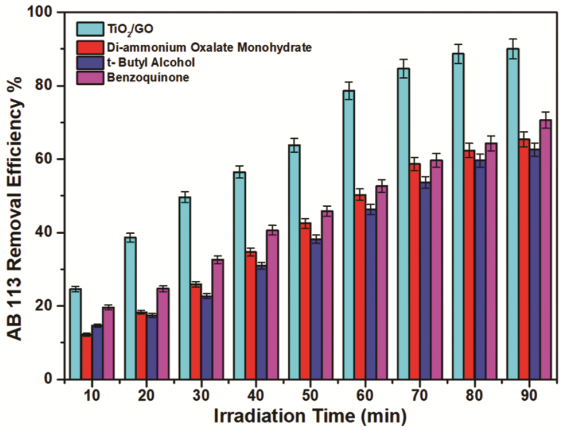

Fig. 8 — Unveiling the impact of scavengers on TiO_2/GO photocatalytic removal of AB 113 dye. Insights into the role of Di-ammonium oxalate monohydrate, t-Butyl alcohol, and Benzoquinone (Dye concentration: 100 mg/L, pH: 7, and scavengers concentration 0.01 M; Error bars represent the standard error of triplicate studies)

wastewater. The trend of these indices during the photodegradation of a dye solution depends on the efficiency of the photocatalytic process and the biodegradability of the intermediates generated during the degradation. The increase in BI from 0.21 ± 0.0105 to 0.416 ± 0.0128, indicated that the photocatalytic process generated more biodegradable intermediates from the complex dye molecules (Fig. 7). This attributed to the degradation of the aromatic structure of the dye molecule and the formation of smaller and more polar compounds that can be readily degraded by microorganisms[9]. The reduction of PI from 6.8 ± 0.238 to 2.13 ± 0.107 mgO_2/L (i.e., 66.18% reduction) indicated that the photocatalytic process was successful in oxidizing the organic compounds in the dye solution. The reduction in PI can be attributed to the photocatalytic oxidation of organic compounds present in the dye solution by reactive oxygen species(hydroxyl radicals (•OH)) generated by the TiO_2/GO composite photocatalyst. This process resulted in a decrease in the amount of oxidizable organic matter, leading to a reduction in the PI[24]. Overall, the experimental results suggested that the photocatalytic pretreatment of AB 113 dye using 0.5 g/L of TiO_2/GO composite photocatalyst was an effective method for enhancing the biodegradability of the dye and reducing the amount of oxidizable organic matter.

Effects of various scavengers

This study investigated the photocatalytic oxidation of AB 113 dye using TiO_2/GO photocatalyst in the presence of different scavengers, including Di-Ammonium oxalate monohydrate, t-Butyl alcohol, and Benzoquinone. The TiO_2/GO photocatalyst exhibited a maximum removal efficiency of 90 ± 2.7%, indicating its excellent photocatalytic activity in the oxidation of AB 113 dye (Fig. 8). The high removal efficiency may be attributed to the synergistic effect of TiO_2 and GO, which can enhance the generation of an •OH radical, leading to an effective removal of the dye. The addition of di-ammonium oxalate monohydrate, a hole scavenger, resulted in a decrease in the removal efficiency to 65.34 ± 2.02%. This suggests that the holes generated in the photocatalytic process played a crucial role in the degradation of the dye, and their removal through the scavenging process[36]. The addition of t-Butyl Alcohol, an •OH radical scavenger, also led to a decrease in removal efficiency to 62.58±1.81%. This indicates that •OH radicals generated during the photocatalytic process were the main species responsible for the degradation of the dye, and their removal through scavenging led to a decrease in the removal efficiency[37]. Furthermore, the addition of Benzoquinone, an electron and superoxide radical ($•O_2^-$) scavenger, resulted in a slight decrease in the removal efficiency to 70.59 ± 2.25%. This suggests that the electrons generated during the photocatalytic process were not the limiting species in the degradation of AB 113 dye. Moreover, superoxide radicals scavenging also exhibited a relatively minor effect on the dye removal efficiency[38]. An •OH radical was relatively more responsible for AB 113 removal in comparison to the holes and superoxide

radicals. Based on the results of scavenger effects on AB 113 removal, the photocatalytic mechanism can be described as follows:

Scheme 1: The formation of electron-hole pairs (h^+/e^-), leading to the generation of reactive species such as hydroxyl radicals (•OH), superoxide radicals ($•O_2^-$), and holes (h^+).

$TiO_2/GO + h\nu \rightarrow e^- + h^+$

$h^+ + H_2O \rightarrow •OH + H^+$

$TiO_2/GO\ (e^-) + O_2 \rightarrow •O_2^-$

Scheme 2: The reactive species attack and oxidize the AB 113 dye molecules.

AB 113 + h^+/e^- + •OH /$•O_2^-$→ CO_2 + H_2O + inorganic byproducts

Scheme 3: Di-ammonium oxalate monohydrate reacts with the holes (h^+) generated on the surface of TiO_2/GO to form ammonium ions and oxalic acid.

h^+ + Di-Ammonium oxalate monohydrate → Oxalic acid + NH_4^+

Scheme 4: t-Butyl Alcohol scavenges hydroxyl radicals, reducing the number of available reactive species for the photocatalytic reaction and inhibiting the photocatalytic activity of TiO_2/GO.

•OH + t-Butyl alcohol → t-Butyl alcohol radicals + H_2O

Scheme 5: Benzoquinoneacts as an electron sink, reducing the number of available electrons for the photocatalytic reaction. This also leads to a decrease in AB 113 removal efficiency.

Benzoquinone + e^- → Hydroquinone

The superoxide radicals react with Benzoquinone to form Benzoquinone semiquinone radicals, which are relatively stable and do not react with other radicals.

$•O_2^-$ + Benzoquinone → Benzoquinone $^{-•}$(Benzoquinone semiquinone radicals)

Recycling of photocatalyst

In this study, the reusability of the TiO_2/GO composite photocatalyst for the removal of AB 113 dye was investigated. TiO_2/GO composite retained its photocatalytic activity up to 5 cycles to remove the dye, albeit with a gradual decrease in the removal efficiency from 90 ± 2.7% to 83.58±2.92% (Fig. 9). This decrease in photocatalytic activity could be attributed to the accumulation of dye molecules on the surface of the photocatalyst over successive cycles. This accumulation could lead to the partial blocking of the active sites of the photocatalyst and hinder the interior diffusion of the dye molecules. As a result, the less effective surface area was available

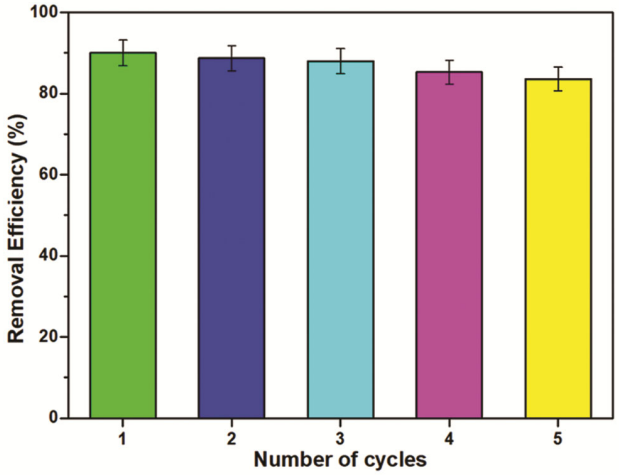

Fig. 9 — Reusability study of TiO_2/GO composite photocatalyst (AB 113 concentration: 100 mg/L, TiO_2/GO dose: 0.5 g/L, and Irradiation time: 90 min). Error bars represent the standard error of triplicate studies

for the photocatalytic degradation of the dye molecules, and subsequently the removal efficiency declined over successive cycles. Furthermore, repeated exposure to the reaction environment and the recovery process can also cause some degree of physical and chemical damage to the composite, leading to a loss of structural integrity and photocatalytic activity. Photocatalyst deactivation also occurred over successive cycles due to the agglomeration of the TiO_2/GO composite. The composite photocatalyst was found to be stable, reusable, and remained its activity in five successive cycles.

Continuous biodegradation of AB 113 in fixed bed bioreactor

The biodegradation of AB 113 dye was investigated using a FBR with varying dye loadings. The biodegradability of the dye was improved (BI~0.4) through preliminary photocatalytic oxidation and became more amenable to biodegradation. As the dye loading increased from 150 mg/L to 700 mg/L, the biodegradation efficiency gradually decreased. For a dye loading of 150 mg/L, with a flow rate of 40 mL/h and a hydraulic retention time (HRT) of 6 days, the FBR achieved a maximum biodegradation efficiency of 95.07 ± 3.09%, 88.36 ± 2.42% COD, and 97.67 ± 3.09% TOC removal (Fig. 10). As the dye loading increased to 200 mg/L, the biodegradation slightly decreased to 93.7 ± 3.04%, with COD and TOC removal percentages of 90.51 ± 2.35% and 96.89 ± 3.06%, respectively, under the same flow rate and extending the HRT to 7 days. This reduction in performance may be attributed to the

higher dye loading, which could have increased the stress on the biodegradation system. Moreover, as the dye loading increased to 400, 500, and 700 mg/L, the FBR was able to steadily recover the dye biodegradation efficiency, demonstrating dye biodegradation efficiencies of 90.3 ± 2.93%, 87.3 ± 2.84%, and 85.03 ± 2.76%, respectively. Remarkably, the FBR was able to withstand the increased loading and maintain its biodegradation performance. Longer HRTs and lower flow rates allowed to increase contact time between the dye molecules and the microorganisms, enhancing the degradation process. The gradual increase in dye loading may have stimulated the growth and activity of dye-degrading microorganisms in the FBR[39]. The presence of higher dye concentrations can act as a substrate for the microbial community, promoting their metabolic activity and improving dye biodegradation efficiency. As the dye loading increased, the biomass within the FBR might have increased and acclimated to the higher dye concentrations[40]. This biomass growth and acclimation could have resulted in enhanced dye degradation capabilities and contributed to the recovery of biodegradation efficiencies. The critical findings of AB 113 biodegradation were highlighted in Table 1. Further, a comparative analysis of combined photocatalytic oxidation and biodegradation of dye wastewater has been described in Table 2.

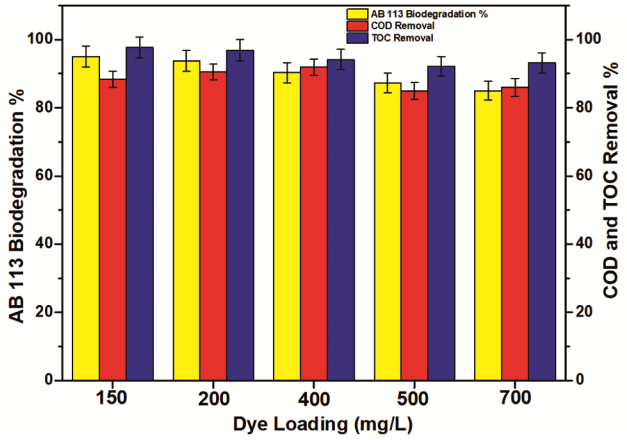

Fig. 10 — Biodegradation performance of the Fixed Bed Bioreactor for AB 113 dye, showing AB 113 biodegradation, COD, and TOC removal percentage at different inlet dye loadings (150-700 mg/L) and hydraulic retention times (6-12 days)

The apparent rate constant k_{app} declined as influent dye loading was increased. This trend suggested one or more of the following at higher loadings: (i) mass-transfer limitations (diffusion into biofilm / onto immobilized cells), (ii) substrate inhibition or toxicity to biofilm microbes at very high dye concentrations, and/or (iii) reduced fraction of readily biodegradable intermediates per unit influent at higher loadings. The decreasing k_{app} supported HRT selection: longer HRTs (up to 12 days) were required at higher loads to maintain acceptable removal. A comparative analysis of combined photocatalytic oxidation and biodegradation of dye wastewater has been highlighted in Table 3.

Biofilm activity and performance

The biodegradation performance of the FBR depended on the metabolic activity of the attached microbial biofilm. The attached biofilm exhibited high biodegradation at low influent concentrations

Table 1 — Summary of Experimental Findings for Acid Blue 113 Dye Loadings in a Fixed Bed Bioreactor

AB 113 Loading (mg/L)	HRT (days)	Final AB 113 Concentration (mg/L)	Flow rate (mL/h)	Initial COD (mg/L)	Final COD (mg/L)	Initial TOC (mg/L)	Final TOC (mg/L)
150	6	7.4± 0.32	40	485.6± 12.8	56.5± 2.1	325.8± 8.5	7.6± 0.28
200	7	12.6± 0.41	40	786.4± 20.4	74.6± 2.4	415.3± 10.9	12.9± 0.33
400	8	38.8± 0.95	35	1316.5± 34.1	105.4± 3.8	824.6± 21.4	48.41± 1.65
500	9	63.5± 1.72	30	1688.3± 43.4	254.5± 6.1	965.8± 25.1	75.71± 2.94
700	12	104.8± 3.15	20	2256.5± 58.7	316.17± 8.2	1428.6± 37.1	97.15± 3.75

Table 2 — A typical illustration of the fitted apparent first-order rate constants using the experimental findings (Eq. 5)

Influent AB-113 (mg/L)	HRT (days)	Effluent (mg/L)	k_{app} (day^{-1})
150	6	7.4 ± 0.32	0.5015
200	7	12.6 ± 0.41	0.3949
400	8	38.8 ± 0.95	0.2916
500	9	63.5 ± 1.72	0.2293
700	12	104.8 ± 3.15	0.1583

Table 3 — A Comprehensive Overview of Integrated Photocatalytic Oxidation-Biodegradation Studies on Diverse Dye Contaminants in Literature

S.N.	Dye	Photocatalyst	Bioreactor and Microorganism	Dye Concentration and %Degradation	References
1.	Acid Blue 113	Anatase TiO_2	Fixed Bed Bioreactor, *Klebsiella michiganensis* strain DP2ZMA43	300 mg/L, 92 ± 2.6 %	9
2.	Direct Black 22	ZnO/Polypyrrole composite	Batch study, Bacterial Consortium	205.15 mg/L, 95.7%	41
3.	Real Textile Wastewater	Anatase TiO_2	Batch Study *Providencia rettgeri* HSL1	Color 75 PCU, 93.33%; Hybrid treatment improved color removal and reduced toxicity; high HRT required due to complex wastewater.	42
4.	Reactive Green 12	TiO_2-impregnated polyester	Batch Reactor Bacterial Consortium present in activated sludge	74.9%	24
5.	Methyl Red	ZnO	*Galactomyces geotrichum* and *Brevibaccilus laterosporus*	500 mg/L, complete degradation	43
6.	Reactive Brilliant Red X-3b	g-C_3N_4-P_{25}	Rhodospirillum, photosynthetic bacteria	94%	44
7.	Ethyl Violet	TiO_2-coated beads	Packed Bed Bioreactor, Proteobacteria phylum	50 mg/L, 98%	45
8.	Textile Wastewater	Anatase TiO_2	Moving bed reactor, Bacterial Consortium	87%	46
9.	Crystal Violet	Anatase TiO_2	Fixed Bed Bioreactor, Phylum Proteobacteria	200 mg/L, 98%	47
10.	Reactive dyes	TiO_2 visible-light photocatalysis	Batch biological degradation	80–85%; Sequential oxidation + biological treatment improved mineralization but limited by photocatalytic efficiency.	48
11.	Acid Blue 113	TiO_2/GO composite	Fixed Bed Bioreactor, *Klebsiella michiganensis* strain DP2ZMA43	700 mg/L, 85.03 ± 2.76%; GO improved visible-light activation and charge separation; FBR improved stability and biodegradation; HRT reduced by 30–50%	Present Study

(150-200 mg/L), indicating effective substrate uptake by the biofilm and higher enzymatic activity. Meanwhile, during high influent loading, i.e., ≥ 500 mg/L, the k_{app} was decreased, demonstrating that *Klebsiella michiganensis* biofilm approached its maximum substrate handling capacity. This could be attributed to either the saturation of active sites or partial inhibition by the degraded intermediate compounds.

Mass Transfer Limitations

Mass transfer could become a vital factor in FBR during the diffusion of the substrate across multiple interfaces, i.e., bulk liquid, boundary layer, and microbial biofilm matrix, before it comes into intimate contact with active microbial cells. The higher influent AB 113 loading was liable for the increased diffusional resistance within the biofilm layers, as reflected in terms of reduced k_{app} values. This phenomenon was responsible for the fact that intrinsic microbial kinetics, rather than substrate diffusion, control the overall mass transfer rate. Moreover, the competitive diffusion pathways could appear with the presence of photocatalytic intermediates or alter the biofilm porosity, thereby further influencing the mass transfer.

Bioreactor hydrodynamics

The hydrodynamic behaviour of the FBR also affects the biodegradation performance. The FBR was allowed to operate under the plug-flow regime; however, the non-ideal behavior, such as dead zone, bypassing, and channeling, could be expected under the regime where the PU foam was irregularly packed. The lower flow rates thereby improved the

Table 4 — Residual toxicity quantification of Acid Blue 113 (200 mg/L), photocatalytically oxidized products, and final biodegraded products using bacterial culture assays at 27 ± 3 °C (Error bars indicate standard error, based on triplicate studies).

S.N.	Sample name	*E. coli* cell viability %	*Bacillus Subtilis* cell viability %
1.	Double distilled Water	100	100
2.	Acid Blue 113	15.3 ± 1.2	19.2 ± 1.4
3.	Photocatalytically oxidized products	45.6 ± 2.2	44.8 ± 2.1
4.	Final biodegraded products	93.1 ± 3.6	97.8 ± 2.4

uniform distribution and maximum efficient contacting of the substrate; while short HRT governed non-ideal flow behaviour, it reduced the effective microbe-substrate contacting. Moreover, the integrated effect of uneven flow distribution and dead zone also affected the oxygen transfer, reduced the microbial activity, and reasonably declined the overall FBR biodegradation efficiency.

Residual toxicity of AB 113, photocatalytically oxidized, and biodegraded products

In this study, the cell viability of *E. coli* and *Bacillus Subtilis* was examined to evaluate the residual toxicity of AB 113, as well as its photocatalytically oxidized (PO) and biodegraded products (BP). Interestingly, the results revealed that the photocatalytic oxidation process significantly improved the cell viability of both bacterial strains compared to the raw AB 113, as depicted in Table 4. Furthermore, the subsequent biodegradation of the photocatalytically oxidized products led to a further reduction in toxicity levels, thereby enabling their safe disposal in the environment. Consequently, the sequential combination of photocatalytic oxidation and biodegradation demonstrated a noteworthy improvement in the cellular viability of both *E. coli* and *Bacillus Subtilis*. These results highlight the potential of this integrated approach in effectively reducing toxicity and enhancing the overall treatment efficacy. According to Ravikumar *et al*.[27], the residual toxicity of Congo red and its treated product was evaluated by assessing the cell viability of *Bacillus* sp. and *Pseudomonas* sp. *Bacillus* sp. and *Pseudomonas* sp. exhibited residual cell viabilities of 60% and 97%, respectively, for treated Congo red dye wastewater. These findings indicate that the biodegradation process contributed to a significant reduction in toxicity, as evidenced by the enhanced cell viability of the bacterial strains.

Conclusion

The synergistic use of photocatalysis and bioremediation is a promising approach for the degradation of organic pollutants, such as dyes from wastewater. The use of Graphene Oxide (GO) as a co-catalyst can enhance the photocatalytic activity of TiO_2 by improving electron transfer and reducing the recombination rate of electron-hole pairs. FTIR and HR-XRD results indicated the successful incorporation of GO into the TiO_2 matrix without any significant alteration in the crystal structure. The smaller band gap (2.73 eV) observed in the TiO_2/GO composite photocatalyst compared to anatase TiO_2 (3.2 eV) can be attributed to the incorporation of GO, which can lead to enhanced light absorption (UV-Visible), reduced charge carrier recombination, increased surface area (12.033 m^2/g), and improved crystallinity. These findings suggest that the TiO_2/GO composite photocatalyst has superior photocatalytic performance compared to anatase TiO_2, making it a promising material for various photocatalytic applications. The incorporation of the FBR enhanced the overall process viability through the mitigation of a massive loading stress of 700 mg/L of AB 113 and exhibited biodegradation efficacy of 85.03 ± 2.76%. The low level of dye loading (150-500 mg/L) was easily biodegraded. A combination of photocatalytic oxidation and biodegradation ensured the almost complete detoxification of treated dye wastewater. The hybrid reactor design shows promising potential for scalability, as both units can be engineered for continuous operation with low energy requirements. With appropriate modification, the photocatalytic step can be driven by solar irradiation, further improving sustainability and reducing operational costs. Future work will focus on validating the system using real industrial wastewater, performing intermediate analysis via HPLC/GC–MS, and optimizing reactor parameters to advance this configuration toward practical field-level application.

Acknowledgments

The authors acknowledge Department of Chemical Engineering, Indian Institute of Technology (BHU), Varanasi, India and Dr. A.P.J. Abdul Kalam

Technical University, Lucknow, Uttar Pradesh, India for providing research and infrastructural facilities to complete this work.

Conflicts of Interest

The authors declare no conflicts of interest.

References

1 Tiwari H, Sonwani R K & Singh R S, Bioremediation of dyes: A brief review of bioreactor performance, *Environ Technol Rev*, 12 (2023) 83.

2 Oladoye P O, Ajiboye T O, Omotola E O & Oyewola O J, Methylene blue dye: Toxicity and potential elimination technology from wastewater, *Results Eng*, 16 (2022) 100678.

3 Islam T, Repon M R, Islam T, Sarwar Z & Rahman M M, Impact of textile dyes on health and ecosystem: A review of structure, causes, and potential solutions, *Environ Sci Pollut Res*, 30 (2022) 9207.

4 Hunge Y M, Yadav A A, Dhodamani A G, Suzuki N, Terashima C, Fujishima A & Mathe V L, Enhanced photocatalytic performance of ultrasound treated GO/TiO_2 composite for photocatalytic degradation of salicylic acid under sunlight illumination, *Ultrason Sonochem*, 61 (2020) 104849.

5 Nidheesh P V, Divyapriya G, Titcho F E & Hamdani M, Treatment of textile wastewater by sulfate radical based advanced oxidation processes, *Sep Purif Technol*, 293 (2022) 121115.

6 Bougdour N, Tiskatine R, Bakas I & Assabbane A, Textile wastewater treatment by peroxydisulfate/Fe(II)/UV: Operating cost evaluation and phytotoxicity studies, *Chem Africa* , 3 (2020) 153.

7 Dhaif-Allah M A H, Taqui S N, Syed U T & Syed A A, Kinetic and isotherm modeling for acid blue 113 dye adsorption onto low-cost nutraceutical industrial fenugreek seed spent, *Appl Water Sci*, 10 (2020) 1.

8 Su X, Li S, Xie M, Tao L, Zhou Y, Xiao Y, Lin H, Chen J & Sun F, Enhancement of polychlorinated biphenyl biodegradation by resuscitation promoting factor (Rpf) and Rpf-responsive bacterial community, *Chemosphere*, 263 (2021) 128283.

9 Tiwari H, Sonwani R K & Singh R S, A comprehensive evaluation of the integrated photocatalytic-fixed bed bioreactor system for the treatment of Acid Blue 113 dye, *Bioresour Technol*, 364 (2022) 128037.

10 Kurniawan T A, Mengting Z, Fu D, Yeap S K, Othman M H D, Avtar R & Ouyang T, Functionalizing TiO_2 with graphene oxide for enhancing photocatalytic degradation of methylene blue (MB) in contaminated wastewater, *J Environ Manag*, 270 (2020) 110871.

11 Dharma H N C, Jaafar J, Widiastuti N, Matsuyama H, Rajabsadeh S, Othman M H D, Rahman M A, Jafri N N M, Suhaimin N S & Nasir A M, A review of titanium dioxide (TiO_2)-based photocatalyst for oilfield-produced water treatment, *Membranes*, 12 (2022) 345.

12 Matsunami D, Yamanaka K, Mizoguchi T & Kojima K, Comparison of photodegradation of methylene blue using various TiO_2 films and WO_3 powders under ultraviolet and visible-light irradiation, *J Photochem Photobiol A Chem*, 369 (2019) 106.

13 Bai H, Zhou J, Zhang H & Tang G , Enhanced adsorbability and photocatalytic activity of TiO_2-graphene composite for polycyclic aromatic hydrocarbons removal in aqueous phase, *Colloids Surfaces B Biointerf*, 150 (2017) 68.

14 Zhang H, Wang X, Li N, Xia J, Meng Q & Lu J, Synthesis and characterization of TiO_2 /graphene oxide nanocomposites for photoreduction of heavy metal ions in reverse osmosis concentrate, *RSC Adv*, 8 (2018) 34241.

15 Lertthanaphol N, Pienutsa N, Chusri K, Sornsuchat T, Chanthara P, Seeharaj P, Lohsoontorn P K & Srinives S, One-step hydrothermal synthesis of precious metal-doped titanium dioxide-graphene oxide composites for photocatalytic conversion of CO_2 to ethanol, *ACS Omega*, 6 (2021) 35769.

16 Rueda-Marquez J J, Levchuk I, Ibañez P F & Sillanpää M, A critical review on application of photocatalysis for toxicity reduction of real wastewaters, *J Clean Prod*, 258 (2020) 120694.

17 Tiwari H, Sonwani R K & Singh R S, Biodegradation and detoxification study of triphenylmethane dye (Brilliant Green) in a recirculating packed-bed bioreactor by bacterial consortium, *Environ*, 45 (2022) 959.

18 Nardjess M, Ridha A, Haythem B, Adala C, Meriem H & Hichem H A, Synthesis, characterization, antimicrobial activity and DNA/BSA interaction of functionalized graphene oxide nanoparticles with 2-(ferrocenyl methylamino) benzonitrile, *J Mol Liq*, 376 (2023) 121374.

19 Hummers W S & Offeman R E, Preparation of graphitic oxide, *J Am Chem Soc*, 80 (1958) 1339.

20 Zeghioud H, Khellaf N, Amrane A, Djelal H, Bouhelassa M, Assadi A A & Rtimi S, Combining photocatalytic process and biological treatment for Reactive Green 12 degradation: Optimization, mineralization, and phytotoxicity with seed germination, *Environ Sci Pollut Res*, 28 (2021) 12490.

21 Rajput A, Rahman M A, Rahman M H & Kuila A, Visible light photocatalytic degradation of organic pollutants in industrial wastewater by engineered TiO_2 nanoparticles, *Biomass Convers Biorefin*, 14 (2023) 17301.

22 Zheng Y, Zhao Y, Su R, An N, Zhang Y, Wei Y & Ma B, A novel method for immobilizing anammox bacteria in polyurethane foam carriers through dewatering, *J Water Process Eng*, 53 (2023) 103738.

23 Ravikumar K V G, Sudakaran S V, Ravichandran K, Pulimi M, Natarajan C & Mukherjee A, Green synthesis of NiFe nano particles using Punica granatum peel extract for tetracycline removal, *J Clean Prod*, 210 (2018) 767.

24 Wu K, Zhou Q, Li Y, Hu X & Ouyang S, Integrating FTIR 2D correlation analyses, regular and omics analyses studies on the interaction and algal toxicity mechanisms between graphene oxide and cadmium, *J Hazard Mater*, 443 (2023) 130298.

25 Lentz L, Mayer D A, Dogenski M & Ferreira S R S, Hybrid aerogels of sodium alginate/graphene oxide as efficient adsorbents for wastewater treatment, *Mater Chem Phys*, 283 (2022) 125981.

26 Krakowiak R, Frankowski R, Mylkie K, Kotkowiak M, Mlynarczyk D T, Dudkowiak A, Stanisz B J, Zgoła-Grześkowiak A, Ziegler-Borowska M & Goslinski T, Titanium(IV) oxide nanoparticles functionalized with various meso-porphyrins for efficient photocatalytic degradation of ibuprofen in UV and visible light, *J Environ Chem Eng*, 10 (2022) 108432.

27 Adly M S, El-Dafrawy S M & El-Hakam S A, Application of nanostructured graphene oxide/titanium dioxide composites for photocatalytic degradation of rhodamine B and acid green 25 dyes, *J Mater Res Technol*, 8 (2019) 5610.

28 Khan S A, Arshad Z, Shahid S, Arshad I, Rizwan K, Sher M & Fatima U, Synthesis of TiO_2/Graphene oxide nanocomposites for their enhanced photocatalytic activity against methylene blue dye and ciprofloxacin, *Compos Part B Eng*, 175 (2019) 107120.

29 Scarpelli F, Mastropietro T F, Poerio T & Godbert N, Mesoporous TiO_2 thin films: State of the Art, *Titan Dioxide Mater Sust Environ*, (2018) 58.

30 Wang D, Li X, Chen J & Tao X, Enhanced photo electrocatalytic activity of reduced graphene oxide/ TiO_2 composite films for dye degradation, *Chem Eng J*, 198 (2012) 547.

31 Martins P M, Ferreira C G, Silva A R, Magalhães B, Alves M M, Pereira L, Marques P A A P, Melle-Franco M & Lanceros-Méndez S, TiO_2/graphene and TiO_2/graphene oxide nanocomposites for photocatalytic applications: A computer modeling and experimental study, *Compos Part B Eng*, 145 (2018) 39.

32 Min Y L, Zhang K, Zhao W, Zheng F C, Chen Y C & Zhang Y G, Enhanced chemical interaction between TiO_2 and graphene oxide for photocatalytic decolorization of methylene blue, *Chem Eng J*, 193 (2012) 203.

33 Behnood R & Sodeifian G, Novel $ZnCo_2O_4$ embedded with S, N-CQDs as efficient visible-light photocatalyst, *J Photochem Photobiol A Chem*, 405 (2021) 112971.

34 Yilmaz M, Mengelizadeh N, Saloot M K, Shahbaksh S & Balarak D, Facile synthesis of Fe_3O_4/ZnO/GO photocatalysts for decolorization of acid blue 113 under solar, visible and UV lights, *Mater Sci Semicond Process*, 144 (2022) 106593.

35 Al-Musawi T J, Mengelizadeh N, Taghavi M, Shehu Z & Balarak D, Capability of copper-nickel ferrite nanoparticles loaded onto multi-walled carbon nanotubes to degrade acid blue 113 dye in the sonophotocatalytic treatment process, *Environ Sci Pollut Res*, 29 (2022) 51703.

36 Chaturvedi A, Rai B N, Singh R S & Jaiswal R P, Comparative toxicity assessment using plant and luminescent bacterial assays after anaerobic treatments of dyeing wastewater in a recirculating fixed bed bioreactor, *J Environ Chem Eng*, 9 (2021) 105466.

37 Sonwani R K, Swain G, Jaiswal R P, Singh R S & Rai B N, Moving bed biofilm reactor with immobilized low-density polyethylene-polypropylene for Congo red dye removal, *Environ Technol Innov*, 23 (2021) 101558.

38 Ceretta M B, Vieira Y, Wolski E A, Foletto E L & Silvestri S, Biological degradation coupled to photocatalysis by ZnO/polypyrrole composite for the treatment of real textile wastewater, *J Water Process Eng*, 35 (2020) 101230.

39 Ambaye T G & Hagos K, Photocatalytic and biological oxidation treatment of real textile wastewater, *Nanotechnol Environ Eng*, 5 (2020) 28.

40 Waghmode T R, Kurade M B, Sapkal R T, Bhosale C H, Jeon B H & Govindwar S P, Sequential photocatalysis and biological treatment for the enhanced degradation of the persistent azo dye methyl red, *J Hazard Mater*, 371 (2019) 115.

41 Zhang X, Wu Y, Xiao G, Tang Z, Wang M, Liu F & Zhu X, Simultaneous photocatalytic and microbial degradation of dye-containing wastewater by a novel g-C_3N_4 -P25 /photosynthetic bacteria composite, *PLOS One*, 12 (2017) 1.

42 Chen C Y, Yen S H & Chung Y C, Combination of photoreactor and packed bed bioreactor for the removal of ethyl violet from wastewater, *Chemosphere*, 117 (2014) 494.

43 Ahmadi M, Amiri P & Amiri N, Combination of TiO_2-photocatalytic process and biological oxidation for the treatment of textile wastewater, *Korean J Chem Eng*, 32 (2015) 1327.

44 Chen C Y, Kuo J T, Yang H A & Chung Y C, A coupled biological and photocatalysis pretreatment system for the removal of crystal violet from wastewater, *Chemosphere*, 92 (2013) 695.